M.A. Izquierdo-Barrientos, C. Sobrino, J.A. Almendros-Ibáñez.(2016) Modeling and experiments of energy storage in a packed bed with PCM, International Journal of Multiphase Flow, Volume 86,pp. 1-9.

DOI: https://doi.org/10.1016/j.ijmultiphaseflow.2016.02.004

Modeling and experiments of energy storage in a packed bed with PCM

M.A. Izquierdo-Barrientos [a, *], C. Sobrino [a], J.A. Almendros-Ibáñez [b, c]

[a] Universidad Carlos III de Madrid, ISE Research Group, Thermal and Fluid Engineering Department, Avda. de la Universidad 30, Leganés, Madrid 28911, Spain

[b] Escuela de Ingenieros Industriales, Dpto. de Mecánica Aplicada e Ingeniería de Proyectos, Castilla-La Mancha University, Campus universitario s/n, 02071 Albacete, Spain

[c] Renewable Energy Research Institute, Section of Solar and Energy Efficiency, C/ de la Investigación s/n, 02071 Albacete, Spain

A B S T R A C T

This work presents a numerical and experimental study of the transient response of a packed bed filled with a granular phase change material (PCM). The proposed numerical model accounts for the progres- sive evolution of the enthalpy with temperature during the phase change rather than using a constant phase change temperature. This temperature-dependent enthalpy is included in the model as an apparent specific heat that is dependent on temperature according to the measurements obtained by differential scanning calorimetry (DSC). The model also includes the energy stored in the wall, which has been shown to have a non-negligible effect in several experimental facilities.

The equations presented are non-dimensionalized, which results in the same differential equation sys- tem regardless of whether a granular PCM or sensible heat storage material is used. In this manner, the same numerical method can be used in cases with or without a granular PCM. Numerical and experimen- tal results are obtained for a conventional granular material (sand) and two commercial granular PCMs with different phase change temperatures. The numerical and experimental heating results exhibit good agreement, and the energy stored in the wall of the bed represents between 8 and 16% of the energy stored in the granular material.

Keywords:
Fixed bed
Phase change material
Energy storage

1. Introduction

The energy storage process reduces the rate mismatch between energy supply and energy demand. Energy can be stored in a material in the form of sensible or latent heat (Cabeza, 2014; Dincer and Rosen, 2002). Water, rock beds and phase change materials (PCMs) are the most suitable media for energy storage. Packed beds are typically used in air-based storage systems. The use of a PCM as the storage medium offers several advantages compared to using sensible heat. PCMs store a large amount of energy in a small volume, and the heat is charged/discharged at a nearly constant temperature (Mehling and Cabeza, 2008).

Waste heat recovery and solar thermal energy systems are primary applications for thermal energy storage (Beasley and Clark, 1984). Waste heat recovery and thermal energy storage can be combined in order to decrease energy consumption, as the energy stored by the storage system can be kept and this energy can be used whenever the industry process needs it (Fernández et al., 2015). Solar air systems, though not as common as water solar systems, can be used in many applications such as space heating or ventilation air heating (Zhao et al., 2011), drying of agricultural products (Chauhan et al., 1996) or regeneration of desiccant cooling systems (Kabeel, 2007; Rady et al., 2009). When using a solar energy source, the inlet fluid temperature will vary continuously with time and hence it is necessary to determine the transient response of the packed bed.

Thermal storage models in packed beds include single- phase models, in which the bed is approximated by a quasi-homogeneous medium (Vortmeyer and Schaefer, 1974), and separate-phase models, which were first studied by Schumann (1929), where two energy conservation equations are obtained for the solid and fluid phases and are coupled by a heat exchange term. Among these models, the concentric dispersion model con- siders a temperature gradient inside the solid spheres (Handley and Heggs, 1969; Kaguei et al., 1977; Xia et al., 2010). Furthermore, one- and two-dimensional models (Beasley and Clark, 1984) can be

* Corresponding author.
E-mail address: maizquie@ing.uc3m.es, mariaizquierdobarrientos@gmail.com (M.A. Izquierdo-Barrientos).

Notation

a	superficial area per unit volume [m^{-1}]
Bi	Biot number [−]
c_p	specific heat [$J \cdot kg^{-1} \cdot K^{-1}$]
d	diameter [m]
E_{stored}	energy stored [J]
Fo	Fourier number [−]
H	height of the bed [m]
h	interphase heat transfer coefficient [$W \cdot m^{-2} \cdot K^{-1}$]
h_w	convective heat transfer coefficient from the bed to the inner surface of the bed [$W \cdot m^{-2} \cdot K^{-1}$]
i	enthalpy [J]
k	thermal conductivity [$W \cdot m^{-1} \cdot K^{-1}$]
$k_{n,x}$	effective thermal conductivity in the axial direction [$W \cdot m^{-1} \cdot K^{-1}$]
k_e^0	stagnation effective thermal conductivity [$W \cdot m^{-1} \cdot K^{-1}$]
m	mass [kg]
Pr	Prandtl number [−]
Re	Reynolds number [−]
T	air temperature [°C]
T_{pc}	phase change temperature [°C]
U	superficial gas velocity [$m \cdot s^{-1}$]
U_∞	Overall heat transfer coefficient [$W \cdot m^{-2} \cdot K^{-1}$]
u	interstitial gas velocity [$m \cdot s^{-1}$]
$\dot{V}$	flow rate [$m^3 \cdot s^{-1}$]

Greek symbols

α	thermal diffusivity [$m^{-2} \cdot s^{-1}$]
ρ	density [$kg \cdot m^{-3}$]
σ_{dp}	standard deviation of the mean particle diameter [m]
θ	solid temperature [°C]
ψ	wall temperature [°C]
ε	void fraction in the bed [−]
Δt	time step [s]
Δx	spatial step [m]

Subscripts

0	ambient/initial
a	air
b	bed
i	internal
in	inlet
o	outer
p	particle
s	solid
w	wall
wi	inner wall
wo	outer wall
x	axial position

distinguished depending on whether the radial temperature profile is considered or not.

A review on the mathematical modeling of PCMs has been published by Dutil et al. (2011). In particular, fixed-grid methods for solid-liquid phase change problems formulate the governing equations for the entire region of the PCM, including the solid and liquid phases (Faghri and Zhang, 2006). The principal problem in these methods is the spatial discretization in the region of the solid-liquid interface. These methods include the following: i) the enthalpy method, in which the energy equation is considered in terms of enthalpy, ii) the equivalent heat capacity method, which converts the latent heat into an equivalent heat capacity of the PCM in the phase change temperature range and iii) the temperature transforming model, which was proposed by Cao and Faghri (1990). The enthalpy method assumes an isothermal phase transition, whereas the equivalent heat capacity and temperature transforming models consider that phase change occurs in a temperature range, where the enthalpy variation with temperature is assumed to be linear. Peng et al. (2014) modeled the transient behavior of a packed bed of PCM capsules for high-temperature thermal storage using molten salts as the heat transfer fluid. The radial temperature distribution inside the capsules was included due to the size of the capsules. Rady (2009a) presented experiments and numerical simulations of the charging process in a small, fixed bed with an internal diameter of 4.5 cm using air as the heat transfer fluid and particles with a smaller particle diameter (1–3 mm), which allowed the temperature variations within the solids to be neglected. Izquierdo-Barrientos et al. (2013) used this material with a smaller particle size (mean diameter of 0.5 mm) in a fluidized bed and observed greater storage efficiencies compared to a typical material, such as sand, in fixed and fluidized beds.

The numerical model presented in this work accounts for the heat stored in the walls of the container. Regarding the phase change process of a pure PCM, other researchers have included the effect of the latent heat of melting using an effective heat capacity within the selected melting range (Farid et al., 1998). In contrast, in the literature of packed beds with PCM it is common to assume a constant phase change temperature (Nithyanandam et al., 2014; Xu et al., 2015) or a linear variation of the enthalpy in a tempera- ture range (Bellan et al., 2015; 2014; Karthikeyan et al., 2014; Peng et al., 2014; 2015). In this work we consider a continuous enthalpy variation with temperature from DSC measurements. The enthalpy data obtained from DSC measurements were interpolated using a cubic spline interpolation.

The materials used in this work and the experimental set-up are described in the following section. Then, the numerical model of the energy storage in a fixed bed is explained. Finally, the experimental and numerical results are compared, and the main conclusions of the work are summarized.

2. Materials and experimental apparatus

The materials used in this study are sand, which is a typical material used for sensible energy storage, and two granular phase-changing composites with different temperature transitions. Both granular PCMs consist of paraffin, which is the PCM, bounded within a secondary supporting structure of SiO_2, which ensures that the paraffin does not leak from the granulate when in liquid form. Table 1 presents several properties of the sand and PCMs, such as the density ρ, thermal conductivity k and mean diameter of the particles $\bar{d}_p$ with its standard deviation σ_{dp}.

Table 1
Material properties.

Material	ρ [kg/m³]	k [W/(m K)]	$\bar{d}_p$ [mm]	σ_{d_p} [mm]
Sand	2648.1	4.2	0.57	0.070
GR50	1512.8	4.0	1.64	0.196
GR80	1618.0	4.0	1.58	0.187

The granular PCMs are commercially available (Rubitherm ®-GR50 and GR80) and similar to those used by Rady (2009a) and Izquierdo-Barrientos et al. (2013) in their studies. The phase change temperature T_{pc} is approximately 50 °C for GR50 and 80 °C for GR80. Those materials are commercialized in two different particle sizes. The finer grade (between 0.2 mm and 0.6 mm) was employed by Izquierdo-Barrientos et al. (2013) in a bubbling fluidized bed because it has a combination of size and density that permits

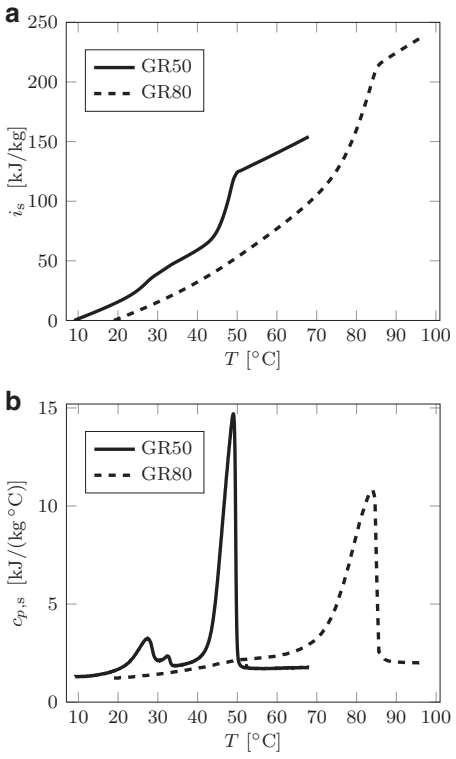

Fig. 1. Enthalpy variation (a) and apparent specific heat (b) as a function of temperature for the granular PCMs, GR50 and GR80.

to operate in the bubbling regime. The coarser grade, used in this work, present a mean particle size of 1.64 mm and 1.58 mm for the GR50 and GR80, respectively. With these sizes, the gas flow rate necessary to fluidize the bed is too high for practical applications and they are more suitable to be used in a fixed bed, with superficial gas velocities under the minimum fluidization velocity. Fig. 1 (a) shows the enthalpy evolution with temperature for the granular PCMs, which was measured by differential scanning calorimetry (DSC) with a slow heating rate of 0.5 °C/min (Rady, 20 09a; 20 09b), which ensures thermal equilibrium in the sample during the DSC measurements. The tests were carried out using a sapphire standard. Rady (2009b) studied the same granular PCM used in this work and he did not observe superheating with heating rates up to 10 °C/min. For the PCM one granule was placed in the DSC sample while for the sand a handful of granules were used. The phase changes of GR50 and GR80 are clearly distinguished at approximately 50 °C and 80 °C, respectively. Fig. 1 (b) presents the variation of the apparent specific heat as a function of temperature obtained from the enthalpy curve (Fig. 1(a)) as follows:

$$c_{p_s} = \frac{\mathrm{d}i_s}{\mathrm{d}T} \tag{1}$$

The specific heat of the sand was also measured, and a mean value of 0.776 kJ/(kg °C) was obtained for the temperature range used in this work.

Fig. 2 shows a scheme of the experimental apparatus used for the heating experiments. The bed consists of a cylindrical tube made from stainless steel with 2-mm-thick walls and filled with particles. The air enters the plenum of the column and flows into the bed through a distribution plate with a thickness of 1.5 mm containing 300 perforations with a diameter of 2 mm, which results in a 3% open area. The instrumentally monitored section of the test apparatus has a height of 500 mm and an internal diameter of $d_i = 200$ mm and is insulated with 2-cm-thick glass wool. The instrumentally monitored section of the test apparatus has a height of 0.5 m and an internal diameter of 0.2 m; and is insulated with 0.02-m-thick glass wool. The bed was filled with material up to a height of $H = 0.5$ m. For the sand, its height was equivalent to a mass of 18 kg because it has a higher density, whereas the mass of both granular PCMs (GR50 and GR80) was approximately

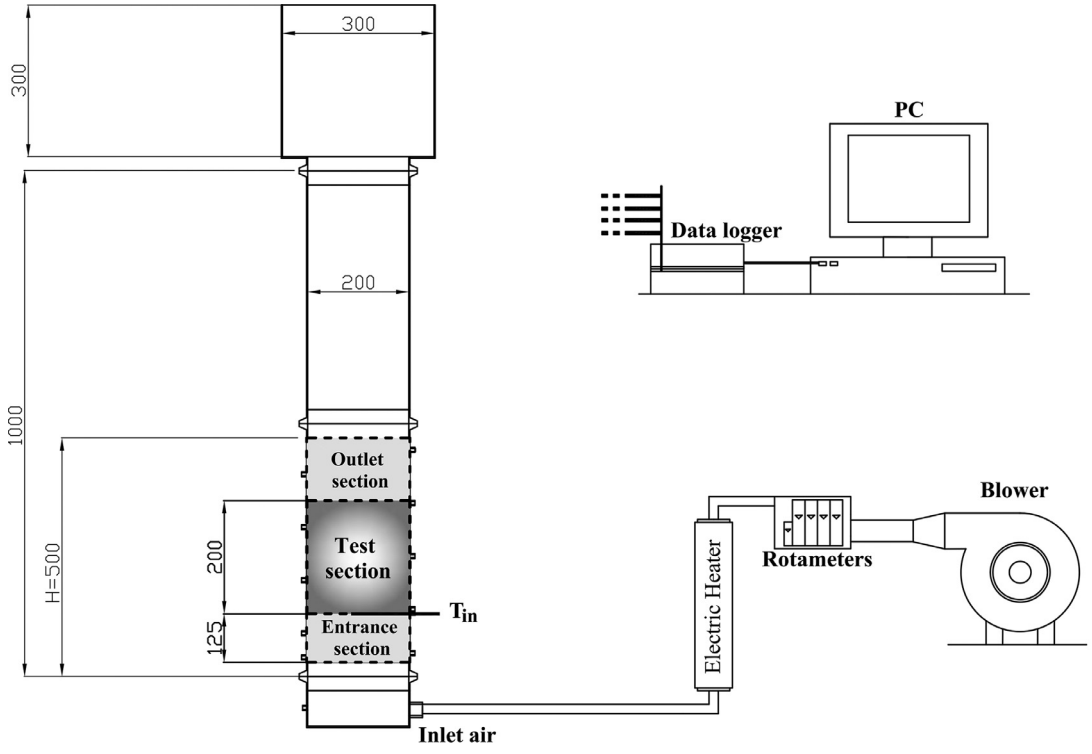

Fig. 2. Scheme of the experimental apparatus. Dimensions in mm.

10 kg. The bed is composed of a 12.5-cm-long entrance section to develop the fluid velocity profile before the fluid enters the test section (Thoméo et al., 2004), where it is measured. The test sec- tion is 20 cm long and corresponds to the numerical domain. The air flow is produced by a blower with a variable mass flow rate and is heated by electrical heaters before flowing into the column. Type K thermocouples with an uncertainty of ± 0.5 °C were used to measure the temperature at specific locations inside the test section and within the plenum chamber.

The bed temperature was uniform and equal to the ambient temperature T_0 at the beginning of every experiment. Before beginning the temperature measurements, the blower is switched on and air is introduced into the column at the desired rate. During this process, the blower heats the air to a temperature greater than the ambient temperature due to the compression process. The entire bed reaches this temperature after approximately 2 h. Once the bed reaches the steady state, the electric heaters are switched on with the required power. The air is heated up to a temperature greater than the T_{pc} of each PCM (65 °C for GR50 and 95 °C for GR80) by regulating the electrical resistance power with a PID controller, which is controlled using the reading of the thermocouple placed at the exit of the electric heaters.

3. Heat transfer model in a packed bed

The proposed two-phase model is explained in the following sections. First, the model is described for a packed bed without phase change in the granular material, and then, the modifications required for the solid phase to include the phase change are described.

3.1. Packed bed model without phase change in the granular material

A one-dimensional time dependent two-phase model is used to describe the mean fluid and solid temperatures in the packed bed. Both, the energy conservation equation for the fluid phase and for the solid phase consider thermal diffusion in axial direction, but the heat transfer from the wall of the tank is only included in the gas equation. The effect of the wall heat capacity has been taken into account so the wall energy conservation equation has been solved together with the fluid and solid equations. This equation includes the axial conduction in the wall and wall energy losses to the ambient. The three conservation equations are

$$\rho_a \varepsilon c_{p,a} \frac{\partial T}{\partial t} = \varepsilon k_{a,x} \frac{\partial^2 T}{\partial x^2} + h a_p (\theta - T) - \rho_a \varepsilon c_{p,a} u \frac{\partial T}{\partial x} - a_{wi,b} h_w (T - \psi), \quad (2)$$

$$\rho_s (1-\varepsilon) c_{p,s} \frac{\partial \theta}{\partial t} = (1-\varepsilon) k_{s,x} \frac{\partial^2 \theta}{\partial x^2} - h a_p (\theta - T), \quad (3)$$

$$\rho_w c_{p,w} \frac{\partial \psi}{\partial t} = k_w \frac{\partial^2 \psi}{\partial x^2} + a_{wi,w} h_w (T - \psi) - a_{wo,w} U_\infty (\psi - T_0), \quad (4)$$

where T is the air temperature, θ is the solid temperature, ψ is the wall temperature, ε is the void fraction in the bed, $a_p = (6(1-\varepsilon))/d_p$ is the superficial particle area per unit of bed volume, $a_{wi,b} = 4/d_i$ is the inner wall surface area per unit of bed volume, $a_{wi,w} = 4 d_i/(d_o^2 - d_i^2)$ is the inner wall surface area per unit volume of bed wall, $a_{wo,w} = 4d_o/(d_o^2 - d_i^2)$ is the outer wall surface area per unit volume of the bed wall and U_∞ is the overall heat transfer coefficient from the outer surface of the wall to the ambient. The air flow passing through the porous bed is considered to be steady and uniform being u the interstitial gas velocity, which is related to the superficial velocity as $U = \varepsilon u$. The correlation proposed by Galloway and Sage (1970) for a particular type of packing and the constants adjusted by Beasley and Clark (1984) were used to calculate the interphase heat transfer coefficient, h. The model proposed by Izquierdo-Barrientos et al. (2014) was used to calculate the convective heat transfer from the bed to the inner surface of the bed, h_w, because the authors validated their results with the same material used in this work.

Table 2
Initial conditions and boundary conditions for Eqs. (2), (3) and (4).

	Gas phase	Solid phase	Wall
Initial condition ($t = 0$)	$T = T_0$	$\theta = T_0$	$\psi = T_0$
Boundary condition ($x = 0$)	$T = T_{in}$	$\frac{\partial^2 \theta}{\partial x^2} = 0$	$\frac{\partial^2 \psi}{\partial x^2} = 0$
Boundary condition ($x = H$)	$\frac{\partial^2 T}{\partial x^2} = 0$	$\frac{\partial^2 \theta}{\partial x^2} = 0$	$\frac{\partial^2 \psi}{\partial x^2} = 0$

The thermal conductivities, $k_{a,x}$ and $k_{s,x}$, are the effective conductivities in the axial direction for the gas and solid phases, respectively. In Eqs. (2) and (3), the conductivities $k_{a,x}$ and $k_{s,x}$ are averaged over the volumes occupied by the gas and particles, respectively. In contrast, in the literature, the effective conductivities are typically averaged over the bed volume. Following the work of Wakao and Kaguei (1982), $k_{a,x}$ can be obtained as follows:

$$k_{a,x} = \begin{cases} 0.7\, k_a & \text{for } Re_p \le 0.8 \\ \dfrac{0.5\, Pr\, Re_p\, k_a}{\varepsilon} & \text{for } Re_p > 0.8 \end{cases} \quad (5)$$

where k_a is the air conductivity, Re_p is the particle Reynolds number based on the superficial velocity and particle diameter and Pr is the Prandtl number. The solid effective conductivity $k_{s,x}$ is calculated from the following relationship:

$$k_{s,x} = \frac{k_e^0 + 0.5\, Pr\, Re_p\, k_a - k_{a,x}\, \varepsilon}{1 - \varepsilon}, \quad (6)$$

where k_e^0 is the stagnation effective thermal conductivity calculated from (Krupiezka, 1967):

$$\frac{k_e^0}{k_a} = \left(\frac{k_s}{k_a}\right)^m \quad \text{with} \quad m = 0.280 - 0.757 \log \varepsilon - 0.057 \log \left(\frac{k_s}{k_a}\right), \quad (7)$$

and k_s is the solid conductivity.

The boundary conditions and initial conditions to solve the differential equation system formed by Eqs. (2), (3) and (4) are summarized in Table 2.

The proposed differential equation system can be transformed into a non-dimensional equation by introducing non-dimensional variables:

$$\hat{T} = \frac{T - T_0}{T_{max} - T_0}, \quad \hat{\theta} = \frac{\theta - T_0}{T_{max} - T_0},$$
$$\hat{\psi} = \frac{\psi - T_0}{T_{max} - T_0}, \quad \hat{t} = t\,\frac{u}{H}, \quad \hat{x} = \frac{x}{H}.$$

With these changes, the non-dimensional temperatures vary between 0, when the temperature is equal to the ambient temperature (minimum temperature) T_0, and 1, when the temperature is equal to T_{max}, which is the maximum temperature of the introduced air.

As a result, the original system is converted into

$$\frac{\partial \hat{T}}{\partial \hat{t}} = Fo_a \frac{\partial^2 \hat{T}}{\partial \hat{x}^2} + Bi_a\, Fo_a (\hat{\theta} - \hat{T}) - \frac{\partial \hat{T}}{\partial \hat{x}} - Bi_{wi,b}\, Fo_a (\hat{T} - \hat{\psi}), \quad (8)$$

$$\frac{\partial \hat{\theta}}{\partial \hat{t}} = Fo_s \frac{\partial^2 \hat{\theta}}{\partial \hat{x}^2} - Bi_s\, Fo_s (\hat{\theta} - \hat{T}), \quad (9)$$

Table 3
Initial conditions and boundary conditions for Eqs. (8), (9) and (10) in non-dimensional form.

	Gas phase	Solid phase	Wall
Initial condition ($\hat{t}=0$)	$\hat{T}=0$	$\hat{\theta}=0$	$\hat{\psi}=0$
Boundary condition ($\hat{x}=0$)	$\hat{T}=1$	$\frac{\partial^2\hat{\theta}}{\partial\hat{x}^2}=0$	$\frac{\partial^2\hat{\psi}}{\partial\hat{x}^2}=0$
Boundary condition ($\hat{x}=1$)	$\frac{\partial^2\hat{T}}{\partial\hat{x}^2}=0$	$\frac{\partial^2\hat{\theta}}{\partial\hat{x}^2}=0$	$\frac{\partial^2\hat{\psi}}{\partial\hat{x}^2}=0$

Table 4
Value of the non-dimensional parameters of Eqs. (8)–(10) for the experimental data of the sand.

Fo_a	Fo_s	Fo_w	Bi_a
1.19×10^{-3}	4.21×10^{-7}	3.19×10^{-5}	1.28×10^{5}
Bi_s	$Bi_{wi,\,b}$	$Bi_{wi,\,w}$	$Bi_{wo,\,w}$
2.10×10^{5}	1.59×10^{3}	3.09×10^{2}	4.77

$$\frac{\partial\hat{\psi}}{\partial\hat{t}}=Fo_w\frac{\partial^2\hat{\psi}}{\partial\hat{x}^2}+Bi_{wi,w}Fo_w(\hat{T}-\hat{\psi})-Bi_{wo,w}Fo_w(\hat{\psi}-\hat{T}_0),\quad(10)$$

where Fo_a, Fo_s and Fo_w represent the Fourier numbers of the air, solid phase and wall, respectively, and Bi corresponds to Biot numbers, which are defined as

$$Fo_a=\frac{\alpha_a}{uH},\quad Fo_s=\frac{\alpha_s}{uH},\quad Fo_w=\frac{\alpha_w}{uH},$$

$$Bi_a=\frac{h\,a_p\,H^2}{k_{a,x}\,\varepsilon},\quad Bi_{wi,b}=\frac{h_w\,a_{wi,b}\,H^2}{k_{a,x}\,\varepsilon},\quad Bi_s=\frac{h\,a_p\,H^2}{k_{s,x}\,(1-\varepsilon)},$$

$$Bi_{wi,w}=\frac{h_w\,a_{wi,w}\,H^2}{k_w},\quad Bi_{wo,w}=\frac{U_\infty\,a_{wo,w}\,H^2}{k_w\,\varepsilon},$$

where α_a and α_s are the thermal diffusivity of the air and solid calculated with their respective effective conductivities, $k_{a,x}$ and $k_{s,x}$. Table 4 show the values of the different non-dimensional numbers of the governing equations for the sand.

The proposed model includes an equation for the wall of the column, which is typically neglected in the packed bed models published in literature, with a few exceptions (Beasley and Clark, 1984). However, the effect of the wall heat capacity has a significant effect in the present bed, as it is 16.2% of the sand heat capacity and 7.6% of the GR50 mean heat capacity for the considered test section. The ratio between the energy stored in the wall and the energy stored in the bed material, assuming that the wall thickness is much smaller than its diameter, can be calculated as follows:

$$\frac{m_w\,c_{p,w}\,\Delta T}{m_s\,c_{p,s}\,\Delta T}\approx\left(\frac{\rho_w\,c_{p,w}}{\rho_s\,c_{p,s}}\right)\left(\frac{4\,t}{d_{int}}\right)\quad(11)$$

where t is the wall thickness. If the volumetric capacity of the bed and the wall material are similar, the ratio between the energy stored in the wall to the energy stored in the bed material decreases linearly with the bed diameter. Thus, the energy stored in the wall is relevant in beds of small sizes, as the one used in this work. For beds of larger diameters, it could be neglected.

The initial conditions and boundary conditions in non-dimensional form are presented in Table 3.

3.2. Packed bed model with phase change in the granular material

When a phase change process is included in the granular mate- rial, the energy equation of the solid phase (Eq. (3)) must be writ- ten in terms of the enthalpy, which yields the following expres- sion:

$$\rho_s(1-\varepsilon)\frac{\partial i_s}{\partial t}=(1-\varepsilon)k_{s,x}\frac{\partial^2\theta}{\partial x^2}-h\,a_p\,(\theta-T),\quad(12)$$

Table 5
Value of the non-dimensional parameters of Eqs. (8), (17) and (10) for the experimental data of the PCM GR50.

Fo_a	$\overline{Fo}_s$	Fo_w	Bi_a
3.90×10^{-3}	2.2×10^{-7}	2.95×10^{-5}	8.02×10^{4}
Bi_s	$Bi_{wi,\,b}$	$Bi_{wi,\,w}$	$Bi_{wo,\,w}$
2.43×10^{5}	4.71×10^{2}	2.02×10^{2}	4.95

where

$$i_s=\int_{T_0}^{T_{max}}c_{p,s}\,d\theta+i_{s_0}\quad(13)$$

is the enthalpy of the solid phase (plotted in Fig. 1 (a)), $c_{p,\,s}$ is the apparent specific heat of the granular PCM (represented in Fig. 1 (b)) and $i_{s\,0}$ is the enthalpy at the reference temperature T_0. Eq. (12) can be non-dimensionalized by introducing the non-dimensional enthalpy

$$\hat{i}_s=\frac{i_s-i_{s_0}}{\bar{c}_{p,s}(T_{max}-T_0)}=\int_0^{\hat{\theta}}\hat{c}_{p,s}\,d\hat{\theta},\quad(14)$$

where

$$\bar{c}_{p,s}=\frac{1}{T_{max}-T_0}\int_{T_0}^{T_{max}}c_{p,s}\,d\theta\quad(15)$$

is the average apparent specific heat in the range of temperatures of the experiments and

$$\hat{c}_{p,s}=\frac{c_{p,s}}{\bar{c}_{p,s}}\quad(16)$$

is a non-dimensional specific heat, which is defined as the ratio of the specific heat at a certain temperature and the average specific heat defined previously. Table 5 summarizes the values of the different non-dimensional numbers of the governing equations for the PCM GR50.

In this manner, the non-dimensional solid equation for the granular material with phase change is

$$\frac{\partial\hat{i}_s}{\partial\hat{t}}=\overline{Fo}_s\frac{\partial^2\hat{\theta}}{\partial\hat{x}^2}-Bi_s\,\overline{Fo}_s(\hat{\theta}-\hat{T}),\quad(17)$$

where $\overline{Fo}_s$ corresponds to the Fourier number defined before, although the average specific heat of the PCM, $\bar{c}_{p,s}$, is used instead of the constant specific heat $c_{p,s}$.

A comparison of Eqs. (9) and (17) demonstrates that both equa- tions have the same form and both non-dimensional variables $\hat{\theta}$ and $\hat{i}_s$ are bounded between 0 and 1. Therefore, the same numerical procedure can be used to solve both equations, as explained in the following section.

3.3. Numerical solution for the heat transfer model

The system of differential equations formed by Eqs. (8), (9) and (10), i.e., when there is no phase change in the granular material, or by Eqs. (8), (10) and (17), i.e., when phase change occurs, can be numerically solved by an explicit finite difference technique. The results are obtained with a discretization length of $\Delta x = 1$ cm and a time step of $\Delta t = 0.\ 1\ \Delta x\ \varepsilon/U$, which ensures convergence of the numerical method. The temporal derivatives were approximated by a fourth-order Runge–Kutta method; the first order spatial derivatives were approximated using backward differences and the second order spatial derivatives were approximated using second-order central differences.

When the solid is a PCM, the enthalpy is calculated at each time step from Eq. (17). Then, the solid temperature is obtained from Fig. 1 (a). The data represented in this figure were interpolated us- ing a cubic spline interpolation.

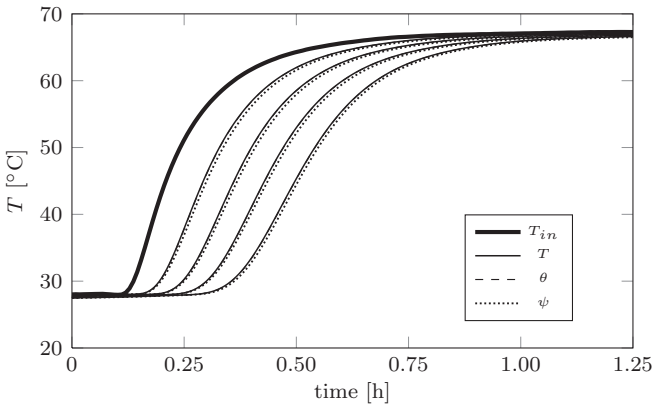

(a) Temperature profiles

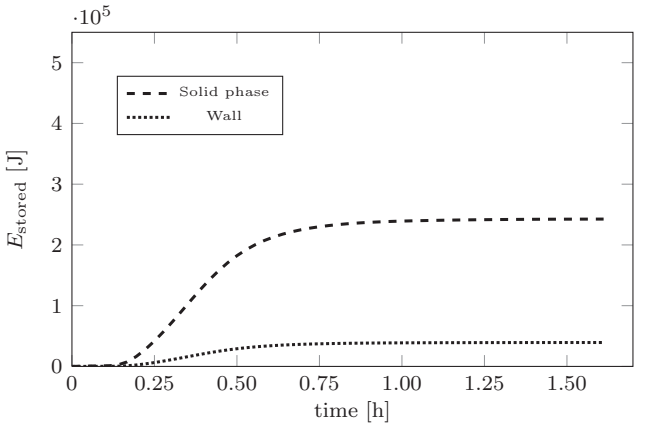

(b) Energy stored

Fig. 3. (a) Temperature profiles modeled for the gas phase T, solid phase θ and wall ψ for the sand at the following axial positions: $x = 5$ cm, $x = 10$ cm, $x = 15$ cm and $x = 20$ cm. $\dot{V} = 450$ l/min and $\varepsilon = 0.4$. (b) Energy stored in the solid phase and the wall.

4. Results and discussion

4.1. Numerical results

Fig. 3 (a) shows the numerical results of the dimensional temperature evolution for the inlet air T_{in}, gas phase T, solid phase θ and wall when the bed is filled with sand. The void fraction selected ε is 0.4, and the chosen flow rate is $\dot{V} = 450$ l/min. The numerical domain is 20 cm long and extends from a height of 12.5 cm above the distributor after the entrance section (Thoméo et al., 2004). The inlet air temperature T_{in} is the temperature mea- sured in the middle of the bed at the beginning of the domain ($x = 0$). The temperature profiles increase progressively along the height of the bed. This behavior is typical of a plug flow system,
where the front travels in the axial direction. The difference between the gas and solid temperature profiles is negligible. Furthermore, the wall temperature has nearly the same profile as the gas and solid, although displaced approximately 1 °C lower.

The energy stored in the material and in the wall is calculated using the following expression:

$$E_{\text{stored}} = \frac{m}{H} \int_{x=0}^{x=H} (i_x - i_0)\, \mathrm{d}x, \tag{18}$$

where H is the height of the test section, m is the mass of the solid phase or the wall for the test section (7.6 and 2.2 kg, respectively), and i_x is the enthalpy calculated at each spatial step.

Fig. 3(b) presents the energy stored in the solid phase (sand) and wall as a function of time. The sand, in the test section,

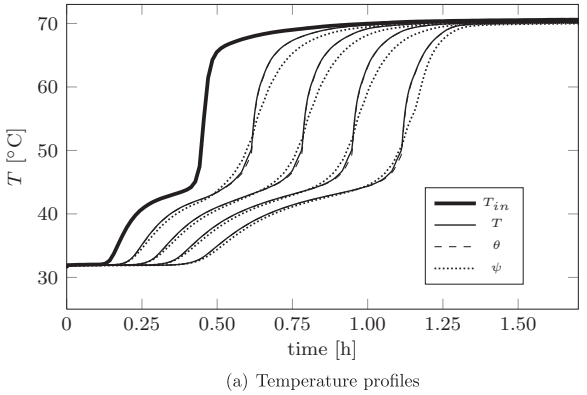

(a) Temperature profiles

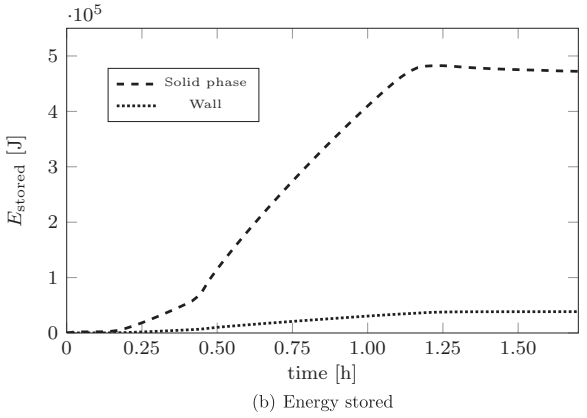

(b) Energy stored

Fig. 4. (a) Temperature profiles modeled for the gas phase T, solid phase θ and wall ψ for GR50 at the following axial positions: $x = 5$ cm, $x = 10$ cm, $x = 15$ cm and $x = 20$ cm. $\dot{V} = 450$ l/min and $\varepsilon = 0.4$. (b) Energy stored in the solid phase and the wall.

stores an estimated 2.4×10^5 J of energy, whereas the wall stores 3.9×10^4 J of energy (16% of the heat stored in the sand).

The numerical results for the temperature profiles and the energy stored when the bed is filled with PCM-GR50 are shown in Fig. 4. In Fig. 4 (a), the temperature profiles plotted are similar to those obtained for sand. The plug flow behavior of the system is preserved, which is characteristic of the thermal storage in packed beds. Moreover, the phase change of the material is revealed with the abrupt change in slope at approximately 47 °C, which corresponds to the phase change of GR50. During this process, the material is able to store energy at a nearly constant temperature. Additionally, different phase change velocities occur along the bed. For example, at a height of $x = 5$ cm, the phase change process occurs in a short interval of time, approximately 0.5 h, whereas at a height of $x = 20$ cm, the phase change process takes nearly 1 h. This difference between phase change velocities is due to the more progressive heating of the particles placed at a greater height as a result of being located far away from the inlet air.

Regarding the energy stored in the solid phase and wall shown in Fig. 4 (b), the energy stored in the wall is 3.9×10^4 J (the same as in the case of the bed with sand) which corresponds to 8.2%
of the energy stored in the PCM, i.e., 4.7×10^5 J, which was calculated for the corresponding mass of the test section (4.2 kg). This percentage, although smaller than that for sand, is still significant and confirms the importance of including the energy conservation equation for the wall.

The evaluation of the energy stored per unit mass for the sand and PCM between the temperature range of 32–70 °C shows that the sand is able to store 3.2×10^4, J/kg, whereas the PCM can store 11.2×10^4 J/kg (3.5-fold more than sand). The percentage of energy stored in latent form (between 40 and 50 °C) for the PCM is 60%,

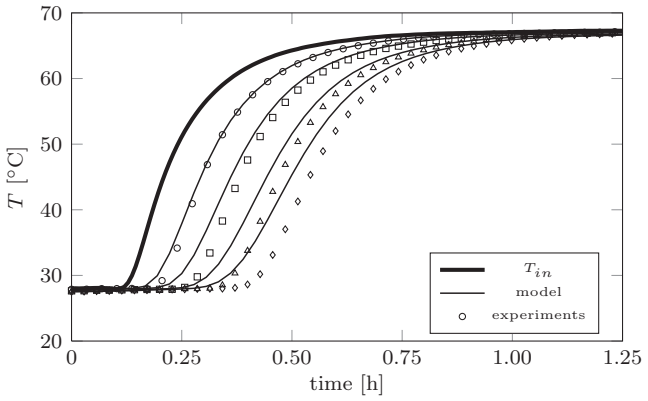

Fig. 5. Measured (markers) and modeled (continuous lines) temperature profiles for sand at the following axial positions: $x = 5$ cm, $x = 10$ cm, $x = 15$ cm and $x = 20$ cm. $\dot{V} = 450$ l/min and $\varepsilon = 0.4$.

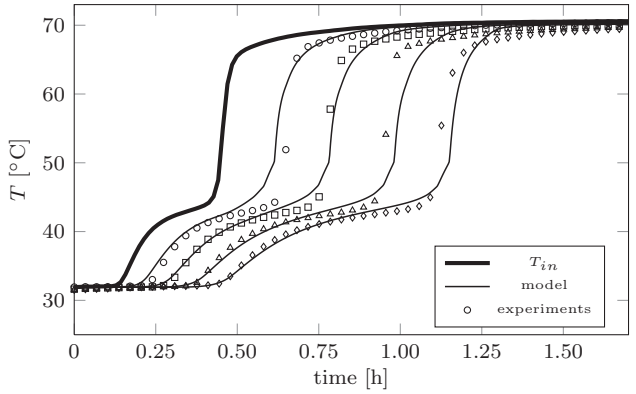

Fig. 6. Measured (markers) and modeled (continuous lines) temperature profiles for GR50 at the following axial positions: $x = 5$ cm, $x = 10$ cm, $x = 15$ cm and $x = 20$ cm. $\dot{V} = 450$ l/min and $\varepsilon = 0.4$.

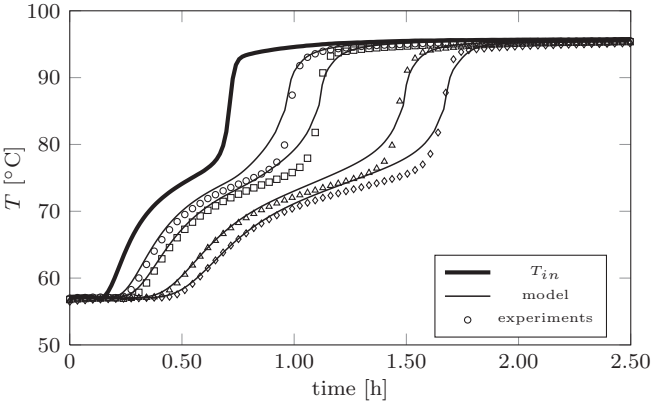

Fig. 7. Measured (markers) and modeled (continuous lines) temperature profiles for GR80 at the following axial positions: $x = 6$ cm, $x = 9.5$ cm, $x = 16.5$ cm and $x = 20$ cm. $\dot{V} = 450$ l/min and $\varepsilon = 0.5$.

which corresponds to 6.7×10^4 J/kg, which is more than the sand can store. This increased storage capacity is due to the ability of the PCM to store energy in a small volume.

Tables 4 and 5 shows the values of the different non-dimensional numbers obtained in the governing equations for the sand and for the PCM GR50, respectively. Note that Fourier numbers are $Fo_s < Fo_w < Fo_a$ due to the differences in the thermal diffusivity of the solid, wall and air. The Biot number $Bi_{wo,w}$ is two orders of magnitude smaller than the other Biot numbers $Bi_{wi,b}$ and $Bi_{wi,w}$ because the global heat transfer coefficient U_∞ is two orders of magnitude smaller than the heat transfer coefficient between the bed and the internal wall, h_w. The Reynolds number, for a flow rate of $\dot{V} = 450$ l/min is equal to 11 for the sand and 25 for the PCM. Note that the correlation used for the interface heat transfer coefficient h (Beasley and Clark, 1984; Galloway and Sage, 1970) is valid for Reynolds numbers up to 5×10^3. The ratio between the thermal conductivity of the solid and the gas is equal to 5.0 for the sand and 7.6 for the PCM. The correlation of Krupiezka (1967) used to obtain the equivalent thermal conductivities was tested for different experimental data ranging from $k_s/k_a = 1$ up to 100. Although the non-dimensional equations of the model are valid for different experimental conditions, such as a liquid instead of a gas, the correlations used to determine the heat transfer coefficients and the equivalente thermal conductivities should be chosen carefully according to the experimental conditions.

4.2. Comparison with the experimental results

Fig. 5 shows the evolution of the experimental temperatures symbolized by markers and the numerical temperature evolution represented by continuous lines for sand. The numerical results were obtained following the procedure detailed in Section 3.3, and the case study is the same as that described in Fig. 3 (a).

A comparison of the experimental and numerical results indicates that the temperature profiles follow the same trend, although they begin to deviate after $x = 5$ cm. This discrepancy may be due to the uncertainty in the calculation of the stagnation effective thermal conductivity k_e^0. If this value is overestimated, the velocity of the heat wave front increases, and hence, the maximum temperature at a certain height in the bed is reached before that in the experiments (Kubie and Broughton, 1975). The rate at which the curves are propagated is controlled by the equivalent thermal conductivity.

The results for GR50 and GR80 for the same flow rate ($\dot{V} = 450$ l/min) are presented in Figs. 6 and 7, respectively.

The abrupt change in slope at approximately 47 °C in Fig. 6 and at approximately 78 °C in Fig. 7 corresponds to the phase change of each material. Due to the phase change, the system requires more time to reach the steady state when heating PCM compared to when using sand. For both PCMs, the plug flow behavior is conserved, and good agreement between the numerical and experimental results is obtained.

According to Arkar and Medved (2005), the shape of the appar- ent specific heat curves depend on the DSC heating rate; in par- ticular, during melting, the peak temperature (temperature peak of the DSC curve) shifts toward the lower temperatures at the lower heating rates, and the peak becomes narrower and higher. The same conclusions were also reached by Rady (2009b). Lázaro et al. (2013) carried out a Round Robin Test to define a procedure for DSC measurements pf PCM to determine the enthalpy temperature curve, concluding that heating and cooling ramps should be very small to ensure the thermal equilibrium of the sample , recommending a maximum of 0.5 K/min. In view of these observations, the small discrepancies between the experimental measurements and model predictions when approaching the peak temperature could be attributed to the PCM material not being in thermal equilibrium, due to the high heating rate experienced by the material during some periods of the experiment.

4.3. Influence of the flow rate

The same experiments were conducted for different flow rates and compared with their corresponding numerical outputs. The results for GR50 for a flow rate of $\dot{V} = 250$ l/min are plotted in Fig. 8, and results similar to that obtained previously were obtained. More time is required to reach steady state and obtain a uniform temperature along the bed when considering a smaller

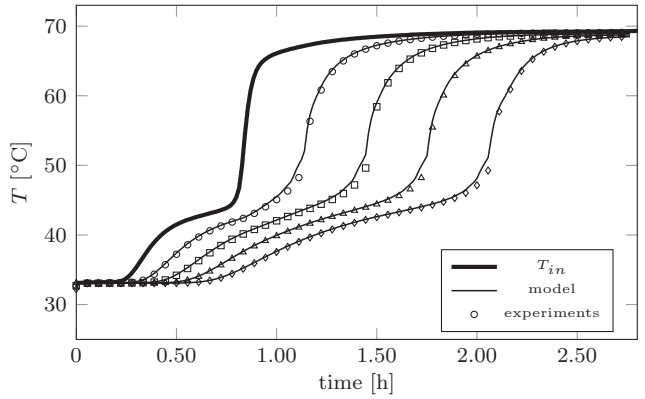

Fig. 8. Temperature profiles for GR50 at the following axial positions: $x = 5$ cm, $x = 10$ cm, $x = 15$ cm and $x = 20$ cm. $\dot{V} = 250$ l/min and $\varepsilon = 0.4$.

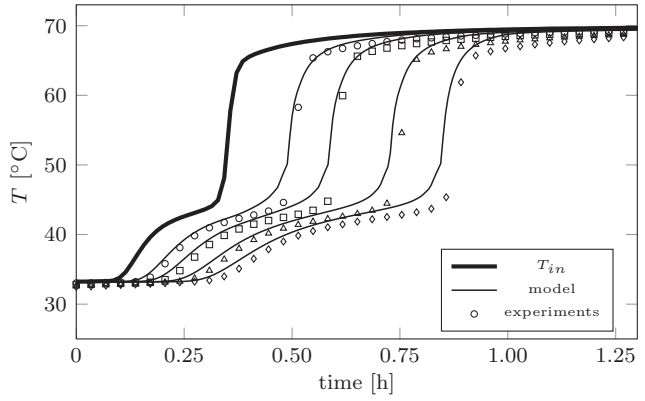

Fig. 9. Temperature profiles for GR50 at the following axial positions: $x = 6$ cm, $x = 10$ cm, $x = 16$ cm and $x = 20$ cm. $\dot{V} = 650$ l/min and $\varepsilon = 0.4$.

flow rate. Moreover, the discrepancies between experimental and model results during the phase change are much smaller than those observed in the previous case at $\dot{V} = 450$ l/min. This is due to the slow heating rate in this experiment, which is smaller than 0.5 °C/min, the heating rate applied is the DSC measurements, that allows the sample to reach the thermal equilibrium.

Fig. 9 presents the results for GR50 at a higher flow rate, $\dot{V} = 650$ l/min. As before, there is nearly no difference between the experimental and numerical results. Thus, the proposed model is suitable for predicting heating temperature profiles for granular PCMs at different flow rates in fixed beds.

5. Conclusions

In this paper, numerical and experimental investigations were performed for a phase change thermal energy storage unit using granulate material. The proposed numerical model accounts for the progressive evolution of the enthalpy with temperature during the phase change and includes the effect of the wall heat capacity.

The equations presented were non-dimensionalized, which results in the same differential equation system regardless of whether the granular material contains PCM or a solid. The model quantifies the energy stored in the wall, which can represent between 8 and 16% of the energy stored in the material.

The transient response of the packed bed was compared with experimental measurements for sand and two phase change granular materials. Discrepancies between experimental and model results for the sand are attributed to the uncertainty in the calculation of the stagnation effective thermal conductivity. The model presents a very good agreement with experimental result for the granular PCM at low air flow rates ($\dot{V} = 250$ l/min). At low flow rates, the heating rate is also low, and close to the heating rate of the DSC measurements (≈ 0.5 °C/min) used to obtain the enthalpy-temperature curves that has been used as an input in the model. Negligible discrepancies are found between experimental and model results during the phase change at higher air flow rate conditions.

Acknowledgments

This work was partially funded by the Spanish Government (Project ENE2010-15403), the regional Government of Castilla-La Mancha (Project PPIC10-0055-4054) and Castilla-La Mancha University (Project GE20101662).

References

Arkar, C., Medved, S., 2005. Influence of accuracy of thermal property data of a phase change material on the result of a numerical model of a packed bed la- tent heat storage with spheres. Thermochim. Acta 438, 192–201.

Beasley, D.E., Clark, J.A., 1984. Transient response of a packed bed for thermal energy storage. Int. J. Heat Mass Tranf. 27, 1659–1669.

Bellan, S., Alam, T.E., González-Aguilar, J., Romero, M., Rahman, M.M., Goswami, D.Y., Stefanakos, E.K., 2015. Numerical and experimental studies on heat transfer characteristics of thermal energy storage system packed with molten salt PCM capsules. Appl. Therm. Eng. 90, 970–979.

Bellan, S., González-Aguilar, J., Romero, M., Rahman, M.M., Goswami, D.Y., Stefanakos, E.K., Couling, D., 2014. Numerical analysis of charging and discharging performance of a thermal energy storage system with encapsulated phase change material. Appl. Therm. Eng. 71, 481–500.

Cabeza, L.F., 2014. Advances in Thermal Energy Storage Systems: Methods and Applications. Elsevier, Cambridge.

Cao, Y., Faghri, A., 1990. A numerical analysis of phase change problems including natural convection. ASME J. Heat Transf. 112, 812–816.

Chauhan, P.M., Choudhury, C., Garg, H.P., 1996. Comparative performance of coriander dryer coupled to solar air heater and solar air-heater-cum-rockbed storage. Appl. Therm. Eng. 16, 475–486.

Dincer, I., Rosen, M.A., 2002. Thermal Energy Storage: Systems and Applications. John Wiley & Sons, England.

Dutil, Y., Rousse, D.R., Salah, N.B., Lassue, S., Zalewski, L., 2011. A review on phase-change materials: mathematical modeling and simulations. Renew. Sust. Energy Rev. 15, 112–130.

Faghri, A., Zhang, Y., 2006. Transport Phenomena in Multiphase Systems, Academic Press, Boston.

Farid, M.M., Hamad, F.A., Abu-Arabi, M., 1998. Melting and solidification in multi-dimensional geometry and presence of more than one interface. Energy Convers. Manag. 39, 809–818.

Fernández, A.I., Barreneche, C., Miró, L., Brückner, S., Cabeza, L.F., 2015. Thermal energy storage (TES) systems using heat from waste. In: Advances in Thermal Energy Storage Systems. In: Woodhead Publishing Series in Energy. Woodhead Publishing, pp. 479–492.

Galloway, T.R., Sage, B.H., 1970. A model of the mechanism of transport in packed, distended, and fluidized beds. Chem. Eng. Sci. 25, 495–516.

Handley, D., Heggs, P.J., 1969. The effect of thermal conductivity of the packing material on transient heat transfer in a fixed bed. Int. J. Heat Mass Transf. 12, 549–570.

Izquierdo-Barrientos, M.A., Sobrino, C., Almendros-Ibáñez, J.A., 2013. Thermal energy storage in a fluidized bed of PCM. Chem. Eng. J. 230, 573–583.

Izquierdo-Barrientos, M.A., Sobrino, C., Almendros-Ibáñez, J.A., 2014. Modeling of the heat transfer coefficient in fixed and fluidized beds with PCM. In: Eurotherm Seminar 99: Advances in Thermal Energy Storage, Lleida.

Kabeel, A.E., 2007. Solar powered air conditioning system using rotary honeycomb desiccant wheel. Renew. Energy 32, 1842–1857.

Kaguei, S., Shiozawa, B., Wakao, N., 1977. Dispersion-concentric model for packed bed heat transfer. Chem. Eng. Sci. 32, 507–513.

Karthikeyan, S., Solomon, G.R., Kumaresan, V., Velraj, R., 2014. Parametric studies on packed bed storage unit filled with PCM encapsulated spherical containers for low temperature solar air heating applications. Energy Convers. Manag. 78, 74–80.

Krupiezka, R., 1967. Analysis of thermal conductivity in granular materials. Int. Chem. Eng. 7, 122–144.

Kubie, J., Broughton, J., 1975. A model of heat transfer in gas fluidized beds. Int. J. Heat Mass Tranf. 18, 289–299.

Lázaro, A., Peñalosa, C., Solé, A., Diarce, G., Haussman, T., Fois, M., Zalba, B., Gshwander, S., Cabeza, L.F., 2013. Intercomparative tests on phase change materials characterization with differential scanning calorimeter. Appl. Energ. 109,415–420.

Mehling, H., Cabeza, L.F., 2008. Heat and Cold Storage With PCM: An up to date introduction into basics and applications. Springer, Berlin.

Nithyanandam, K., Pitchumani, R., Mathur, A., 2 0 1 4 . Analysis of a latent thermocline storage system with encapsulated phase change materials for concentrating so- lar power. Appl. Energy 113, 1446–1460.

Peng, H., Dong, H., Ling, X., 2014. Thermal investigation of PCM-based high temperature thermal energy storage in packed bed. Energy Convers. Manag. 81, 420–427.
Peng, H., Li, R., Ling, X., Dong, H., 2015. Modeling on heat storage performance of compressed air in a packed bed system. Appl. Energy 160, 1–9.
Rady, M., 2009a. Granular phase change materials for thermal energy storage: experiments and numerical simulations. Appl. Therm. Eng. 29, 3149–3159.
Rady, M., 2009b. Study of phase changing characteristics of granular composites using differential scanning calorimetry. Energy Convers. Manag. 50, 1210–1217.
Rady, M., Huzayyin, A., Arquis, E., Monneyron, P., Lebot, C., Palomo, E., 2009. Study of heat and mass transfer in a dehumidifying desiccant bed with macro-encapsulated phase change materials. Renew. Energ. 34, 718–726.
Schumann, T.E.W., 1929. Heat transfer: a liquid flowing through a porous prism. J. Frankl. Inst. 208, 405–416.
Thoméo, J.C., Rouiller, C.O., Freire, J., 2004. Experimental analysis of heat transfer in packed beds with air flow. Ind. Eng. Chem. Res. 43, 4140–4148.
Vortmeyer, D., Schaefer, R.J., 1974. Equivalence of one- and two-phase models for heat transfer processes in packed beds: one dimensional theory. Chem. Eng. Sci. 29, 485–491.
Wakao, N., Kaguei, S., 1982. Heat and mass transfer in packed beds. Gordon and Braech.
Xia, L., Zhang, P., Wang, R.Z., 2010. Numerical heat transfer analysis of the packed bed latent heat storage system based on an effective packed bed model. Energy 35, 2022–2032.
Xu, B., Li, P., Chan, C., Tumilowicz, E., 2015. General volume sizing strategy for thermal storage system using phase change material for concentrated solar thermal power plant. Appl. Energy 140, 256–268.
Zhao, D.L., Li, Y., Dai, Y.J., Wang, R.Z., 2011. Optimal study of a solar air heating system with pebble bed energy storage. Energy Convers. Manag. 52, 2392–2400.